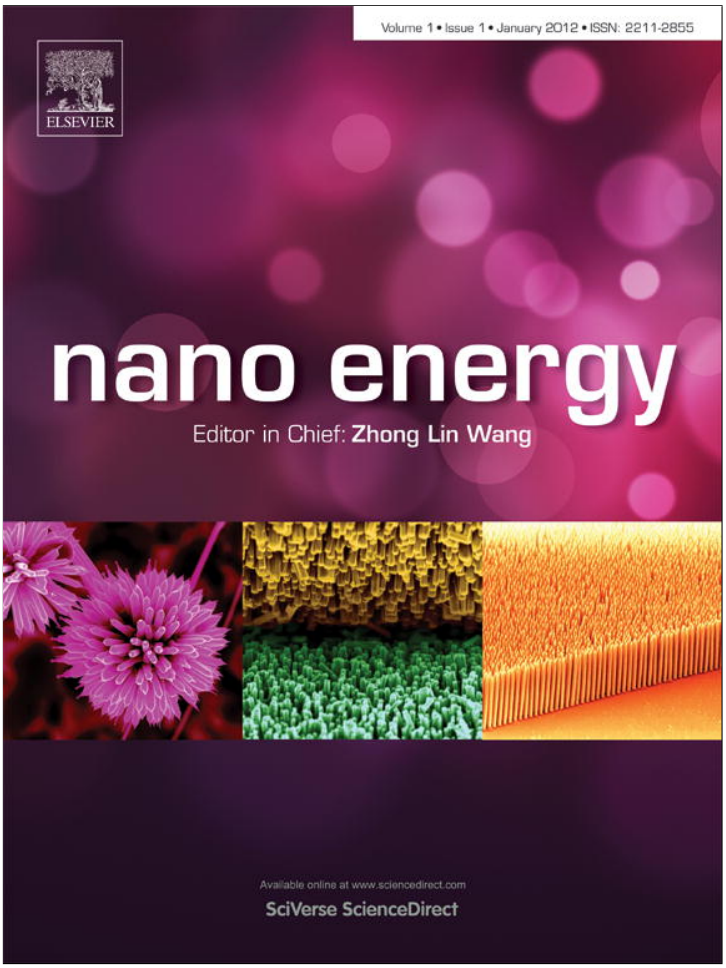

Nano Energy (2012) 1, 176–182

Available online at www.sciencedirect.com

SciVerse ScienceDirect

journal homepage: www.elsevier.com/locate/nanoenergy

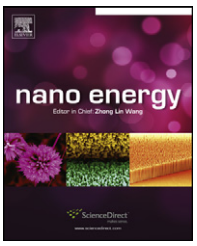

RAPID COMMUNICATION

Optical-fiber/TiO_2-nanowire-arrays hybrid structures with tubular counterelectrode for dye-sensitized solar cell ☆

Wenxi Guo[a,b], Chen Xu[a], Guang Zhu[a], Caofeng Pan[a], Changjian Lin[b,*], Zhong Lin Wang[a,]**

[a] *School of Material Science and Engineering, Georgia Institute of Technology, Georgia 30332, USA*
[b] *State Key Laboratory of Physical Chemistry of Solid Surfaces, College of Chemistry and Chemical Engineering, Xiamen University, Xiamen 361005, China*

Received 30 September 2011; accepted 30 September 2011
Available online 17 October 2011

KEYWORDS
TiO_2 nanowire;
Optical fiber;
Tubular counterelectrode;
Dye-sensitized solar cell

Abstract
We have developed an innovative structure for enhancing the performance of the fiber based 3D DSSC by integrating optical-fiber/TiO_2-nanowire-arrays hybrid structures with cylindrical counterelectrodes. The TiO_2 nanowire arrays are grown on the optical fiber using liquid phase deposition method and platinum is coated on the inwall of stainless steel capillary tubes using electroless deposition. The 3D DSSC is made by sheathering the tube on the fiber structure. In comparison to planar illumination geometry, the efficiency for the 3D structure has been enhanced by a factor of 3.6. An absolute efficiency of 6% has been demonstrated at an optimal length of TiO_2 NWs (12 μm). This study demonstrates a new methodology for building flexible and high-efficient fiber based 3D solar cells that can be expanded to concentrating solar cells.

Introduction

Searching for renewable and ''green''-energy resources is one of the most urgent challenges to the sustainable development of human civilization with the threat of global warming and energy crises [1–6]. As one of the most promising renewable energy resources for sustainable development of the future, dye-sensitized solar cells (DSSCs) have received intensive attention [7–10]. A conversion efficiency of more than 11% [11,12] had been obtained for the photoanode that consists of TiO_2 nanocrystal thin film covered by a monolayer of dye molecules. However, high charge recombination rate and relatively low speed transport of the electrons in the devices remain as barriers for improving overall efficiency [13,14]. In order to solve these problems, efforts have been made to improve the

☆ Electronic Supplementary Information (ESI) available: See DOI: 10.1039/b000000x/.

* Corresponding author.
** Corresponding author. Tel.: +1 404 894 8008; fax: +1 404 384 3852.
E-mail addresses: cjlin@xmu.edu.cn (C. Lin), zhong.wang@mse.gatech.edu, zlwang@gatech.edu (Z.L. Wang).

2211-2855/$ - see front matter © 2011 Elsevier Ltd. All rights reserved.
doi:10.1016/j.nanoen.2011.09.003

transport speed of electrons using one-dimensional (1-D) TiO_2 nano-arrays as photoanodes [10,15–20]. But, due to the smaller surface area compared to that of a nanoparticle structured film, the 1-D TiO_2 nano-arrays structured solar cells are still of low efficiency. To effectively take the advantages offered by the enhanced electron transport property and the surface area, the concept of three-dimensional (3-D) DSSC was proposed [21–25]. Typically, such a 3-D DSSC is based on optical fibers or other waveguide substrates, which are advantageous because they allow light to have multiple interactions with the dye molecules adsorbed on the nanowire (NW) surface without increasing the electron transport distance. A fiber-shaped organic photovoltaic device has been fabricated using multimode optical fibers by constructing concentric thin films, which has demonstrated an energy conversion efficiency of 0.6% under parallel-to-axial illumination [21]. Recently, a 3D DSSC based on the optical fiber–ZnO NW hybrid structure has been investigated and a 3.3% efficiency was obtained by using rectangular fibers and ZnO NWs [23]. Compared to the case of light illumination normal to the fiber axis from the outside of the device, the internal axial illumination enhances the energy conversion efficiency by a factor of up to six for the same device. Although optical fiber based 3D structure is an excellent approach for DSSC, it is still difficult to be applied in liquid DSSC due to the geometry of the planar electrode located at one side of the fiber, which is both poor in contact and difficult to be sealed up, even using a rectangular fiber to enhance contact area between the fiber and the flat Pt electrode for higher efficiency [23]. Moreover, it is well-known that ZnO lacks stability in an acid dye solution and it may form a Zn^{2+}/dye complex on the surface, which seriously restricts the performance of DSSCs [26–28].

In this paper, we have made two innovative improvements on the 3D DSSC. First, instead of ZnO NWs, TiO_2 NWs are fabricated on the optical fibers using liquid phase deposition method while preserving the hybrid structure. Then, the planar counter electrode is replaced by a cylindrical electrode that is sheathed on the optical fiber structure for effective collection of charges. About 6% full sun efficiency has been achieved using this configuration, which is 22% higher than the efficiency received using rutile TiO_2 NWs on a flat FTO substrate [15,16], and 71% higher than that produced using ordered TiO_2 nanotube arrays transformed from ZnO template on TCO glass substrate [20,29,30].

For this study, TiO_2 NWs are prepared on the optical fiber as photoanode. The design principle is shown in Fig. 1. First, a thin layer of ITO and ZnO nanoparticles are deposited on the optical fiber in sequence. Then, vertical aligned TiO_2 NWs are synthesized on optical fibers using the ZnO NWs as a template and liquid phase deposition (LPD) method [20,30]. In the application of 3D DSSCs, light will enter from the axial direction inside the fiber and experience multiple internal reflections along the fiber. We note that ITO layer on the optical fiber not only serves as conductive layer, but also as a high-refractive-index material that allows light to escape the fiber and enter the DSSC. Because the refractive index increases from the quartz fiber core (~1.45), to ITO (2.0) and to anatase TiO_2 (~2.55), the layered structure guarantees that light could escape into the dye from the waveguide [23].

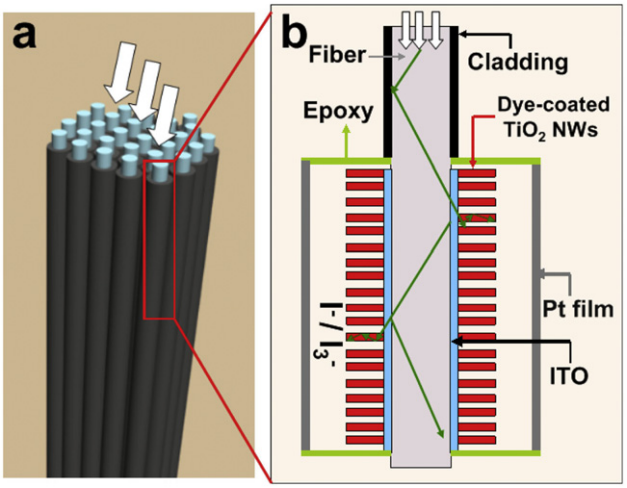

Figure 1 Design and principle of a three-dimensional DSSC. (a) TiO_2 NWs grow vertically on the fiber surface for 3D DSSC; (b) detailed structure of the 3D DSSC.

Experimental

Photoanode preparation

Firstly, the ETFE (ethylene tetrafluoroethylene) jacket of optical fibers provided by OFS Optics (HCS 200) is mechanically stripped and the polymer cladding (HCS) is removed with acetone. Then, the fibers are ultrasonically cleaned in acetone, water, and ethanol consecutively. Next, a layer of 300 nm thick of ITO and 50 nm ZnO are deposited on fibers by radio frequency (RF) magnetron sputtering at room temperature. The samples are parallelly placed on a rotating sample stage and two-step sputter is introduced for uniform coverage of all surfaces. Secondly, ZnO NWs are synthesized by a wet-chemical method in a Pyrex glass bottle containing 20 mM zinc chloride (Aldrich) and 20 mM hexamine (Fluka) at 95 °C for 16 h in a Yamato convection box oven. Aspect ratios were controlled by adding (0–5 mL in 100 mL solutions) 28% ammonium hydroxide (Aldrich). All chemicals are reagent grade. Samples are rinsed with water and ethanol and air-dried at 95 °C for 12 h. Finally, the prepared ZnO NWs on fiber are immersed in a mixed aqueous solution containing 0.075 M $(NH_4)_2TiF_6$ and 0.2 M H_3BO_3 at room temperature for 3–5 h. The resultant TiO_2 NWs are calcined in air at 450 °C for 2 h to form anatase and increase crystallinity. Fiber tips are cleaved with a corning diamond fiber cleaver that ensures efficient light coupling into the fiber.

Counter electrode preparation

For flat Pt electrode, a Pt layer is evaporated on a precleaned glass substrate with a Ti adhesion layer that serves as the counterelectrode. For cylindrical, tube-shaped electrode, Pt layer is deposited on the inwall of the tube using the chemical method introduced by Chen et al. [31]. Firstly, stainless steel tubes with inner diameters of ~500 μm are ultrasonic cleaned in acetone, ethanol, and deionized (DI) water consecutively. Next, the inner wall of tube is etched by continuous feed of 30 wt% H_2SO_4 etching

solution at 60 °C for 5 min followed by cleaning. The Pt layer is deposited on the inner wall of tubes by continuous feed of a plating solution that is composed of 156 mg/L H_2PtCl_6 and 4% HCl at 80 °C for different time. After deposition, the tubes are transferred into furnace and calcined in air at 385 °C for 15 min to remove the impurities.

3D DSSC fabrication

The TiO_2 NWs are sensitized in a 0.3 mM cisbis(isothiocyanato)bis(2,2′-bipyridyl-4,4′-dicarboxylato)-ruthenium(II)bis-tetrabutylammonium dye (N-719 as received from Solaronix) solution in dry ethanol for 24 h [32]. For parallel to axis (PA) illumination case, the working electrode fiber coated with sensitized TiO_2 NWs is placed in parallel with the Pt film counterelectrode. The internal space of the device is filled with a liquid electrolyte (0.5 M LiI, 50 mM I2, 0.5 M 4-tertbutylpyridine in 3-methoxypropionitrile (Fluka)) by the capillary effect. The entire cell is fully packaged and shielded to prevent light leakage. For tubular counter electrode (TC) case, we insert an optical fiber into a stainless steel capillary tube (SSCT); then the liquid electrolyte is injected into the tube by the capillary effect. Finally, the end at one side of the tube is sealed up by flow-mix epoxy and black tape, and only the end of the optical fiber is exposed for the entrance of light. So, the cell's aperture area for receiving the light is taken as the cross sectional area of the optical fiber.

3D DSSC output measurements

The solar cell is irradiated using a solar simulator (300 W Model 91160, Newport) with an AM 1.5 spectrum distribution calibrated against a NREL reference cell to accurately simulate a full-sun intensity (100 mW/cm^2). The *J*–*V* curve is measured under three configurations: light illumination normal to the fiber axis (NA; Fig. 3a case 1) and parallel to the fiber axis (PA; Fig. 3a case 2). For the PA case, the optical fiber is completely shielded by black scotch tape except the end at which the light is guided into the fiber. Then, changing the incident light angle by rotating the cell continually until the short circuit current reaches the maximum [33,34]. Based on the illuminate ways, the different cell's aperture area for receiving the light is defined as follows: for NA case, the projected area of the photo-anode is (optical fiber diameter + 2 × TiO_2 film thickness) × the anode's optical length (2–3 cm). For PA case and TC case, the projected area of the photo-anode is the cross sectional area of the optical fiber.

Results and discussion

Structural and morphological characterization

As can be seen in scanning electron microscopy (SEM) images shown in Fig. 2a and b, vertical and dense ZnO nanowire arrays of ~14 μm in length are grow radially around the optical fiber. Subsequently, these ZnO NWs are converted into TiO_2 NWs via liquid-phase TiO_2 deposition [20,29]. Simultaneously, ZnO is dissolved by immersing the arrays in an aqueous solution

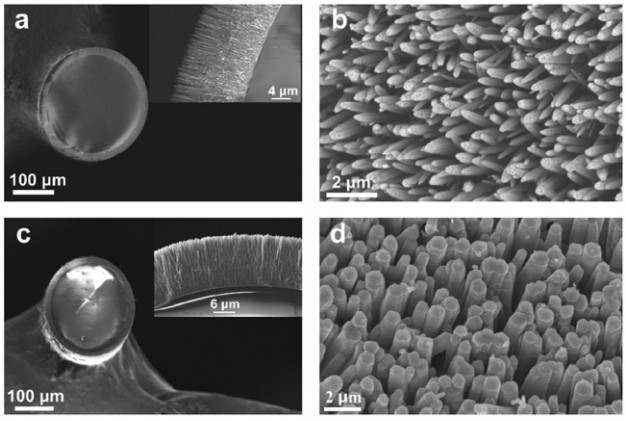

Figure 2 SEM images of ZnO and TiO_2 nanowire arrays on the optical fiber: (a) and (b) are cross section and top views of ZnO nanowire arrays; (c) and (d) are cross section and top views of TiO_2 nanowire arrays. The inserts are the corresponding high-magnified SEM images.

consisting of ammonium hexafluorotitanate and boric acid, forming TiO_2 NWs. Fig. 2c and d shows the morphology of the as-prepared TiO_2 NW arrays, with little shorter length and larger diameter compared to those of ZnO NW arrays. After calcination at 450 °C for 2 h, uniform and polycrystalline TiO_2 NWs film with some cracks on it is obtained, which is shown in Fig. S1a (online supporting information). We scrape the film and the bottom views of the TiO_2 NWs as shown in Fig. S1b and c (online supporting information). From the SEM images, porous structure consisting of lots of bottom-open tubes is observed. Furthermore, a hollow-core structure of the NWs can be observed from the TEM images shown in Fig. S1d (online supporting information). In order to figure out the content of ZnO left in the obtained film, Energy dispersive X-ray spectroscopy (EDX) shows the contents of Zn in different locations for the NWs after 5 h conversion process (see in the Fig. S2 and Table S1 in the online supporting information), indicating that all the ZnO upper has been dissolved while only 3.22 at% and 3.75 at% Zn are respectively left in the middle and bottom of the NWs. The chemical reactions of the formation of TiO_2 NWs may be described as the follows [20,35,36]:

$$TiF_6^{2-} + 2H_2O = TiO_2 + 6F^- + 4H^+ \quad (1)$$

$$H_3BO_3 + 4HF = HBF_4 + 3H_2O \quad (2)$$

$$ZnO + 2H^+ = Zn^{2+} + H_2O \quad (3)$$

Comparison between NA case and PA case

To characterize the performance of a TiO_2 NWs/optical fiber 3D DSSC, a cell was constructed by assembling an individual cylindrical optical fiber in parallel with a planary Pt counterelectrode. TiO_2 NWs with lengths of approximately 12 μm are synthesized on a quartz fiber with a diameter of 200 μm. Two typical configurations are considered: light illumination is normal to the fiber axis (NA) and parallel to the fiber axis (PA), as shown in Fig. 3a (insets). For the PA case, careful measurements were taken in order to eliminate light leakage at the fiber entrance and accurately calculate the illumination cross-sectional area. The plot of current density against voltage (*J*–*V* curve) shows an open

circuit voltage V_{OC}, short-circuit current density J_{SC}, fill factor *FF*, and energy conversion efficiency $\eta = FF*V_{OC}*J_{SC}/P_{in}$, where P_{in} is the incident light power density. It is apparent that the efficiency in the PA case is higher than that in the NA case. To characterize the enhancement in energy conversion efficiency, the efficiency enhancement factor EEF is introduced as the ratio of power efficiencies in the PA and NA cases, $EEF = \eta_{PA}/\eta_{NA}$. According to the *J*-*V* curves of the DSSC, which was shown in Fig. 3a, different performances were observed. In the NA case, J_{SC}=0.87 mA/cm^2, V_{OC}=0.64 V, *FF*=0.32, η_{NA}=0.18%, while in the PA case, J_{SC}=6.18 mA/cm^2, V_{OC}=0.53 V, *FF*=0.49, η_{PA}=1.60%. The current density in the PA case is much larger than that in the NA case, which is due to internal reflections inside the fiber, creating multiple opportunities for energy conversion at the interfaces when light illuminates the fiber from one end along the axial direction. In comparison, the open-circuit voltage in the PA case is lower than NA case, since the local light intensity at the TiO_2-dye interface is lower in the PA case than in the NA case, which has been proved by our previous work [22,23]. By converting the 2D DSSC to 3D DSSC, the EEF ranges from 4 to 9 according to our comprehensive study on eight DSSCs (Fig. 3b), which is consistent with and better than our previously reported work for ZnO [22,23]. It provides the proof that the 3D structure is favorable for the absorption of light for multiple internal reflections in the fiber.

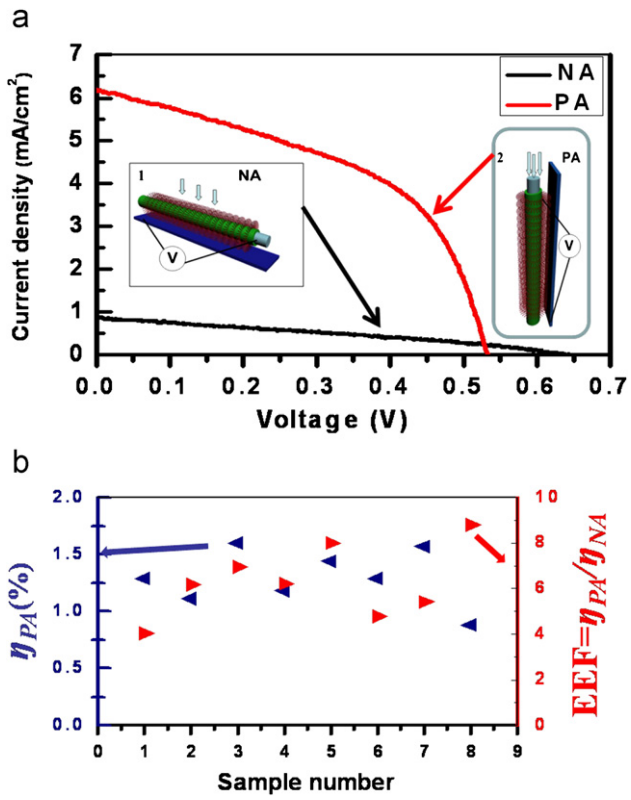

Figure 3 (a) *J*-*V* curves of the DSSC under one full-sun illumination (AM 1.5 illumination, 100 mW/cm^2). The illumination is (1) normal to the fiber axis (NA; 2D case) and (2) parallel to the fiber axis (PA; 3D case). (b) Plot of EEF and the corresponding energy conversion efficiencies for eight 3D DSSCs.

Effect of the length of TiO_2 NWs on optical fiber

In order to investigate the influence of TiO_2 NWs thickness on the 3D solar cell performance, TiO_2 NWs with different thickness are fabricated on optical fibers. The current-voltage characteristics of four typical cells are shown in Fig. 4a. From the characteristic *I*-*V* curve it can be seen that the η_{PA} increases when the thickness of TiO_2 NWs increases from 2 μm to 12 μm, but decreases when further increasing the thickness of TiO_2 NWs, reaching a peak value at the 12 μm length, as shown in the Fig. 4. For 2-6 μm length TiO_2 NWs, the low efficiency and short-circuit current may be attributed to the low surface area for the adsorption of dye. For the 6-12 μm length TiO_2 NWs, the surface area increases while on increasing the TiO_2 NWs thickness, and more dye is adsorbed onto the NWs surfaces allowing an increase in light harvesting. However, when the thickness of the NWs is more than 12 μm, the efficiency decreases from 0.88% to 0.63% and the V_{OC} decreases from 0.53 V to 0.51 V. The reasons why the thickness >12 μm length TiO_2 NWs did not show better performance are may be as follows: Firstly, the longer NWs form a thicker continuous film on the fiber surface, which may diffusely scatter the light before reaching the dye molecules. We also observe that ZnO NWs are very difficult to transform into TiO_2 NWs completely when the lengths are over 25 μm, because several micrometers ZnO nanoparticles will form on the bottom of the ZnO NW arrays by homogeneous nucleation, which cannot be

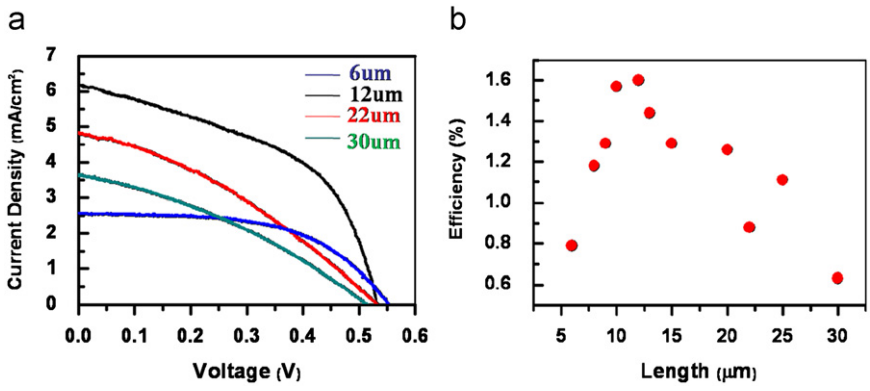

Figure 4 (a) *J*-*V* curves of the DSSC based on TiO_2 NWs with different length (PA; 3D case). (b) Plot of the corresponding energy conversion efficiencies versus lengths for eleven 3D DSSCs (PA case).

easily transformed into TiO_2. Secondly, there are cracks in the base structure with long TiO_2 NWs, which will be the recombination centers for photogenerated electrons. Finally, for TiO_2 nanotubes, although the electron diffusion length is about 100 μm [17], the optimum thickness of TiO_2 nanotubes/nanowires is far less than this length, which may be due to unavoidably increasing diameter, probability of interfacial recombination and degree of disorder while increasing the thickness of the film. In addition, for 3D solar cell, due to the lower local incident light intensity at the TiO_2-dye interface, the optimum length of TiO_2 NWs will be even smaller than 2D solar cell.

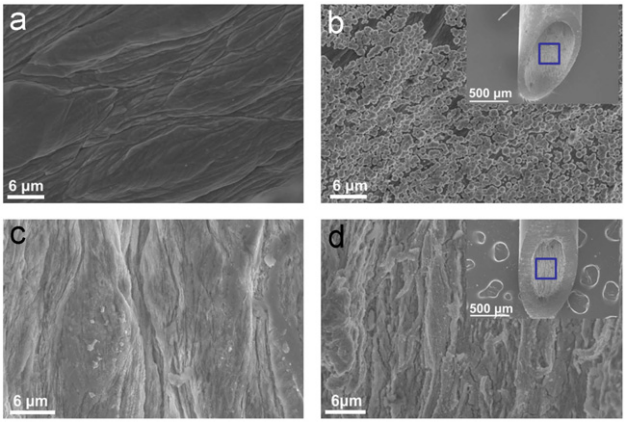

Figure 5 SEM micrographs showing the surface microstructures of the inwall of SSCT (a) before and (c) after etching treatment, and the Pt layer on the inwall (d) with and (b) without etching pretreatment, the inserts are the corresponding low-magnified SEM images.

3D DSSC with tubular counter electrode

For the TiO_2 NWs based 3D DSSCs, the absolute efficiency is about 1.6% due to the flat Pt electrode that fails to collect the charges generated at the other side of the fiber (Fig. 3a). To overcome this difficulty, a Pt-coated tubular electrode is introduced as the counter electrode that sheathes the fiber. Such a cylindrical shell electrode not only increases the effective contact area for collection the charges, but also makes the cell easier to be packaged. Moreover, according to the previous work [37–39], stainless steel has good stability in liquid electrolytes containing I^-/I_3^- redox species. They also found that using stainless steel as the counter electrode for large-scale DSSCs produced higher fill factors and energy conversion efficiencies than DSSCs using glass based substrates, and this result is due to the lower sheet resistance of metals. In addition, SSCT is a very good flexible material for future application in flexible DSSCs [40].

In the present study, the counter electrode was prepared by electroless deposition of Pt on inwall of a stainless steel capillary tube (internal 0.5 mm, outer 0.6 mm,). Before deposition of Pt layer, the inner wall of the tube was etched by continuous feed of 30 wt% H_2SO_4 etching solution at 60 °C for

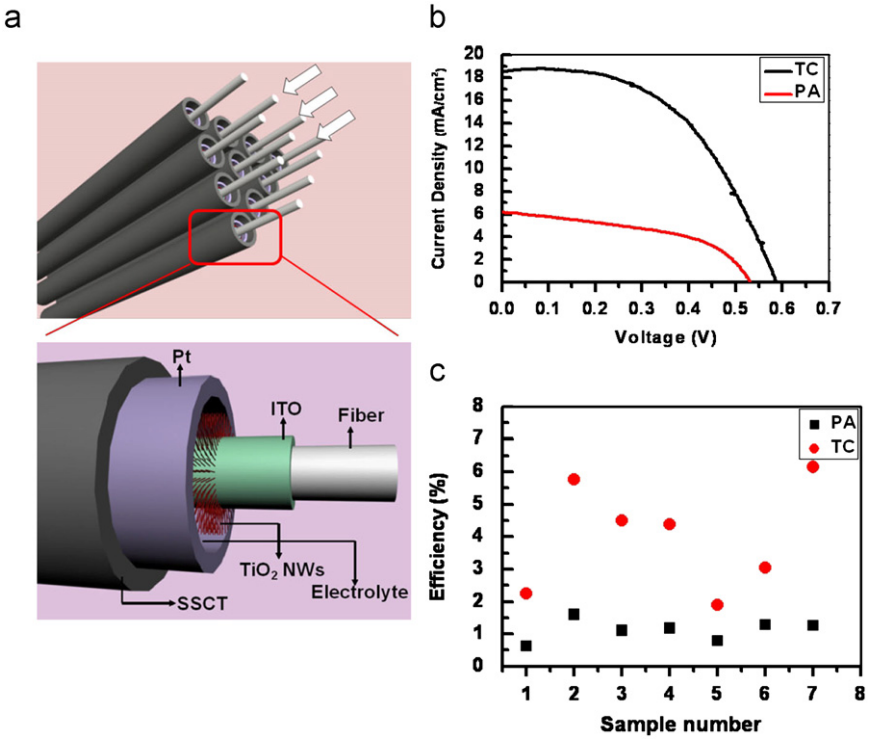

Figure 6 (a) Schematic diagram showing the device structure of optical fiber based 3D DSSCs with capillary tube as counter electrode (the device is totally sealed by epoxy and black scotch tape except the end at which the light is guided into the fiber). (b) Cylindrical optical fiber-based 3D DSSC and its performance. The illumination is parallel to the fiber axis without (PA case) and (c) with (TC case) capillary as counter electrode. (d) Plot of the corresponding energy conversion efficiencies for seven 3D DSSCs (PA case and TC case).

5–10 min. The morphology of the inwall surface of SSCT before and after etching is shown in Fig. 5a and c. the etching process shows at least two benefits for the deposition of Pt layer: on one hand, very rough and porous surface morphology will be obtained after etching, which is favor for the deposition of Pt and enhancing the surface area of counter electrode; on the other hand, the etching process primarily removes iron and chromium from the stainless steel, and the surface of the stainless steel becomes rich in nickel. Much more uniform and density Pt layer can be obtained on etched surface because nickel has higher activity for the chemical deposition of Pt [31]. Following the etching process, Pt layer was deposited on the inwall of the tubes by continuous feed of a plating solution that is composed of 156 mg/L H_2PtCl_6 and 4% HCl at 80 °C for different time. The surface morphologies of Pt layer on the inwall with and without etching pretreatment are show in the Fig. 5b and d, respectively. It can be easily observed that a uniform and dense Pt layer is obtained on the pretreated inner wall while the discontinuous layer forms on the inwall without etching. The contents of Pt before deposition and after deposition are also confirmed by EDX spectra which are shown in the Fig. S3a and b (online supporting information).

An optical fiber covered with 12 μm long TiO_2 NWs is used as the photoanode in assembling a tubular-shaped DSSC. We inserted N719-sensitized TiO_2 NWs-optical fiber hybrid structure in a capillary tube. Next, the electrolyte is injected into the tube by the capillary effect. To accurately compare the performances of the same fiber with planar electrode (PA case) and the tubular electrode (TC case), all the fibers are sealed up except the end at which the light is introduced into the fiber. The *J–V* curve (see Fig. 6b) shows that the current density increased sharply from 6.18 to 18.50 mA/cm^2, and the efficiency reached 5.64% in the TC case. Fig. 6c shows the corresponding energy conversion efficiencies for fourteen such 3D DSSCs, an enhancement factor of 3.6 in efficiency is obtained by replacing the planar electrode with the cylindrical electrode.

Conclusions

In summary, we have developed two innovative approaches for enhancing the performance of the fiber based 3D DSSC. The first step is to replace the ZnO NWs grown on fiber optical fiber by TiO_2 NWs. The full sun efficiencies have been increased up to 1.6% with the use of planar electrode. TiO_2 NWs with length of 12 μm is optimum for obtaining the optimized efficiency. The second approach is to replace the planar electrode by a cylindrical electrode, leading to an increase of the energy conversion efficiency by a factor of 3.6. An absolute efficiency of 6% has been demonstrated. This study expands the 3D DSSC from ZnO based to TiO_2 based materials with largely improved efficiency.

Acknowledgment

Thanks for the support of NSF, BES DOE. WXG thanks the support from the Chinese Scholars Council, and CJL gratefully acknowledges the financial supports from the National Natural Science Foundation of China (51072170, 21021002).

Appendix A. Supplementary materials

Supplementary data associated with this article can be found in the online version at doi:10.1016/j.nanoen.2011.09.003.

References

[1] X.D. Wang, J.H. Song, J. Liu, Z.L. Wang, Science 316 (2007) 102–105.
[2] Z.L. Wang, J.H. Song, Science 312 (2006) 242–246.
[3] Z.L. Wang, Scientific American 298 (2008) 82–87.
[4] B.Z. Tian, X.L. Zheng, T.J. Kempa, Y. Fang, N.F. Yu, G.H. Yu, J.L. Huang, C.M. Lieber, Nature 449 (2007) 885–888.
[5] C.F. Pan, Y. Fang, H. Wu, M. Ahmad, Z.X. Luo, Q.A. Li, J.B. Xie, X.X. Yan, L.H. Wu, Z.L. Wang, J. Zhu, Advanced Materials 22 (2010) 5388–5392.
[6] C.F. Pan, H. Wu, C. Wang, B. Wang, L. Zhang, Z.D. Cheng, P. Hu, W. Pan, Z.Y. Zhou, X. Yang, J. Zhu, Advanced Materials 20 (2008) 1644–1648.
[7] B. Oregan, M. Gratzel, Nature 353 (1991) 737–740.
[8] U. Bach, D. Lupo, P. Comte, J.E. Moser, F. Weissortel, J. Salbeck, H. Spreitzer, M. Gratzel, Nature 395 (1998) 583–585.
[9] N.G. Park, K. Lee, S.W. Park, M.J. Ko, K. Kim, Nature Materials 8 (2009) 665–671.
[10] O.K. Varghese, M. Paulose, C.A. Grimes, Nature Nanotechnology 4 (2009) 592–597.
[11] M. Gratzel, Journal of Photochemistry and Photobiology A 168 (2004) 235.
[12] M. Gratzel, Chemical Research 42 (2009) 1788–1798.
[13] S. Nakade, Y. Saito, W. Kubo, T. Kitamura, Y. Wada, S. Yanagida, Journal of Physical Chemistry B 107 (2003) 8607–8611.
[14] L.M. Peter, J.R. Jennings, Journal of Physical Chemistry C 111 (2007) 16100–16104.
[15] C.A. Grimes, X.J. Feng, K. Shankar, O.K. Varghese, M. Paulose, T.J. Latempa, Nano Letters 8 (2008) 3781–3786.
[16] E.S. Aydil, B. Liu, Journal of the American Chemical Society 131 (2009) 3985–3990.
[17] L.M. Peter, J.R. Jennings, A. Ghicov, P. Schmuki, A.B. Walker, Journal of the American Chemical Society 130 (2008) 13364–13372.
[18] G.K. Mor, K. Shankar, M. Paulose, O.K. Varghese, C.A. Grimes, Nano Letters 6 (2006) 215–218.
[19] M. Law, L.E. Greene, J.C. Johnson, R. Saykally, P.D. Yang, Nature Materials 4 (2005) 455–459.
[20] D. Gao, C.K. Xu, P.H. Shin, L.L. Cao, J.M. Wu, Chem. Mater. 22 (2010) 143–148.
[21] D.L. Carroll, J.W. Liu, M.A.G. Namboothiry, Applied Physics Letters (2007) 90.
[22] Y.G. Wei, C. Xu, S. Xu, C. Li, W.Z. Wu, Z.L. Wang, Nano Letters 10 (2010) 2092–2096.
[23] B. Weintraub, Y.G. Wei, Z.L. Wang, Angewandte Chemie International Edition 48 (2009) 8981–8985.
[24] S. Ruhle, Z. Tachan, A. Zaban, Solar Energy Materials and Solar Cells 94 (2010) 317–322.
[25] Y. Fu, Z. Lu, S. Hou, H. Wu, D. Wang, C. Zhang, Z. Chu, X. Cai, X. Fan, Z.L. Wang, D.C. Zou, Energy and Environmental Science, 2011, doi:10.1039/C1EE01427G.
[26] X.M. Li, J.J. Qiu, F.W. Zhuge, X.Y. Gan, X.D. Gao, W.Z. He, S.J. Park, H.K. Kim, Y.H. Hwang, Nanotechnology (2010) 21.
[27] K. Westermark, H. Rensmo, A.C. Lees, J.G. Vos, H. Siegbahn, Journal of Physical Chemistry B 106 (2002) 10108–10113.
[28] K. Keis, C. Bauer, G. Boschloo, A. Hagfeldt, K. Westermark, H. Rensmo, H. Siegbahn, Journal of Photochemistry and Photobiology A 148 (2002) 57–64.
[29] S. Yoshikawa, P. Charoensirithavorn, Y. Ogomi, T. Sagawa, S. Hayase, Journal of Crystal Growth 311 (2009) 757–759.
[30] D.Y. Kim, S.I. Na, S.S. Kim, W.K. Hong, J.W. Park, J. Jo, Y.C. Nah, T. Lee, Electrochimica Acta 53 (2008) 2560–2566.

[31] C.M. Chen, C.H. Chen, T.C. Wei, Electrochimica Acta 55 (2010) 1687–1695.
[32] P. Schmuki, P. Roy, D. Kim, K. Lee, E. Spiecker, Nanoscale 2 (2010) 45–59.
[33] Y. Li, W. Zhou, D. Xue, J.W. Liu, E.D. Peterson, W.Y. Nie, D.L. Carroll, Physics Letters (2009) 95.
[34] S. Curran, J. Talla, S. Dias, J. Dewald, Journal of Applied Physics (2008) 104.
[35] J.H. Lee, I.C. Leu, M.C. Hsu, Y.W. Chung, M.H. Hon, Journal of Physical Chemistry B 109 (2005) 13056–13059.
[36] S. Deki, S. Iizuka, A. Horie, M. Mizuhata, Kajinami, Chemistry of Materials 16 (2004) 1747–1750.
[37] M. Toivola, F. Ahlskog, P. Lund, Solar Energy Materials and Solar Cells 90 (2006) 2881–2893.
[38] T.L. Ma, X.M. Fang, M. Akiyama, K. Inoue, H. Noma, E. Abe, Journal of Electroanalytical Chemistry 574 (2004) 77–83.
[39] X.M. Fang, T.L. Ma, M. Akiyama, G.Q. Guan, S. Tsunematsu, E. Abe, Thin Solid Films 472 (2005) 242–245.
[40] M. Toivola, J. Halme, K. Miettunen, K. Aitola, P.D. Lund, International Journal of Energy Research 33 (2009) 1145–1160.

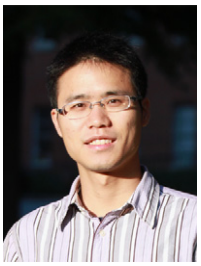

Mr. Wenxi Guo received his Bachelor's degree in College of Chemistry and Chemical Engineering at Xiamen University in 2008. He is a Ph.D. candidate in College of Chemistry and Chemical Engineering at Xiamen University and also a visiting student in the School of Materials Science and Engineering at Georgia Institute of Technology now. His research interests include ZnO and TiO_2 nanomaterials synthesis, materials characterization, and dye-sensitize solar cells.

Chen Xu is a Ph.D. candidate in the School of Materials Science and Engineering at Georgia Institute of Technology. His research mainly focuses on integration of nanowire-based devices including piezoelectric-nanowire-based devices and nano-enabled photovoltaic devices and developing novel processes for the integration of top-down and bottom-up approaches in nanoscale devices. He received his BS in Electrical Engineering from Fudan University. cxu9@mail.gatech.edu

Mr. Guang Zhu received his Bachelor's degree in Materials Science and Engineering from Beijing University of Chemical Technology in 2004. He was enrolled into the Ph.D. program in Materials Science and Engineering at Georgia Institute of Technology. His research interests include nanomaterials synthesis, materials characterization, and microelectronics for renewable energy generation based on semiconducting nanomaterials.

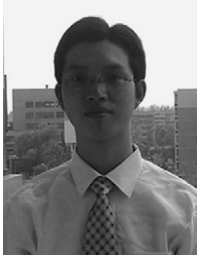

Caofeng Pan received his B.S. degree (2005) and Ph.D. (2010) in Materials Science and Engineering from Tsinghua University, China. He is currently a research scientist in the group of Professor Zhong Lin Wang at the Georgia Institute of Technology. His main research interests focus on the fields of nano-power source (such as nanofuel cell, nano-biofuel cell, and nanogenerator), hybrid nanogenerators, piezotronics, and piezo-phototronics for fabricating new electronic and optoelectronic devices.

Changjian Lin obtained his Ph.D. degree from College of Chemistry and Chemical Enginering at Xiamen University in 2008. From 1987 to 1990 he worked as a postdoctor in National Institute of Standards and Technology in USA. Currently, he is a distinguished professor in chemistry at Xiamen University. His current research concentrates on the area of electrochemical methods, corrosion and protection, surface modification, nanomaterials electrochemistry, and nano-bio-electrochemistry. Particular interests in various scanning micro-probes for in situ imaging electrochemical inhomogeneities at the metal surfaces and metal/solution interfaces, surface modifications for improving the corrosion resistance and inside into the passivity on metal surface, and the advanced materials in electrochemical aspects, such as biomaterials, nanomaterials, environmental and energy materials. He has published 270 peer-reviewed papers and 25 patents, and won several awards and honors including Second Prize of the Progress in Science and Technology, State Education Ministry (1988), First Prize of the Progress in Science and Technology in Xiamen (1995), Outstanding Winner of Doctoral Degree in China (1991), National Foundation for the Outstanding Young Scientists (1996), Second Prize of Innovation, State Education Ministry (2002, 2003), Second Prize of the Progress in Science and Technology, Fujian Province Government (2004).

Dr. Zhong Lin (ZL) Wang is the Hightower Chair in Materials Science and Engineering, Regents' Professor, Engineering Distinguished Professor and Director, Center for Nanostructure Characterization, at Georgia Tech. Dr. Wang is a foreign member of the Chinese Academy of Sciences fellow of American Physical Society, fellow of AAAS, fellow of Microscopy Society of America, and fellow of Materials Research Society. Dr. Wang has been awarded the MRS Medal in 2011 from Materials Research Society and Burton Medal from Microscopy Society of America. He has made original and innovative contributions to the synthesis, discovery, characterization, and understanding of fundamental physical properties of oxide nanobelts and nanowires, as well as applications of nanowires in energy sciences, electronics, optoelectronics, and biological science. His discovery and breakthroughs in developing nanogenerators establish the principle and technological road map for harvesting mechanical energy from environment and biological systems for powering a personal electronics. His research on self-powered nanosystems has inspired the worldwide effort in academia and industry for studying energy for micro—nano-systems, which is now a distinct disciplinary in energy research and future sensor networks. He coined and pioneered the field of piezo-tronics and piezo-phototronics by introducing piezoelectric potential gated charge transport process in fabricating new electronic and optoelectronic devices. This breakthrough by redesign CMOS transistor has important applications in smart MEMS/NEMS, nanorobotics, human—electronics interface, and sensors. Dr. Wang's publications have been cited for over 45,000 times. The *H*-index of his citations is 102. Details can be found at: http://www.nanoscience.gatech.edu.